

Cite this article as: Pu Dongmei, Chen Xianhua, Ye Junliu, et al. Microstructure and Mechanical Properties of $Ti_p/AM60$ Composites[J]. Rare Metal Materials and Engineering, 2022, 51(12): 4436-4445.

ARTICLE

Microstructure and Mechanical Properties of $Ti_p/AM60$ Composites

Pu Dongmei¹, Chen Xianhua^{1,2}, Ye Junliu¹, Liu Chunquan¹, Zhao Jie¹, Pan Fusheng^{1,2}

¹ College of Materials Science & Engineering, Chongqing University, Chongqing 400045, China; ² National Engineering Research Center for Magnesium Alloys, Chongqing University, Chongqing 400045, China

Abstract: AM60 magnesium alloys reinforced with titanium particles (Ti_p) were prepared by semi-solid stirring assisted ultrasonic vibration at different stirring speeds. The microstructure results show that the grain size increases after adding Ti particles. The Al_8Mn_3 phase is precipitated at the interface of Ti particles, and the interface structure between Ti particles and Mg matrix is a coherent interface. The tensile test results show that the strength of $Ti_p/AM60$ composites is higher than that of the AM60 matrix. With increasing the stirring speed from 300 r/min to 900 r/min, the UTS and elongation both increase first and then decrease. The UTS and elongation of $Ti_p/AM60$ composites reach the maximum of 183 MPa and 14.3%, respectively, when the stirring speed is 600 r/min. The UTS is increased by 15% and elongation is increased by 51% compared with those of the AM60 matrix alloy.

Key words: magnesium matrix composites; Ti particles; semi-solid stirring; tensile strength

With the increasingly severe energy and environmental issues, the significance of lightweight becomes even more critical in the manufacturing sector. Magnesium is one of the most abundant light metal elements on the earth. The crustal abundance of magnesium is about 2%. Its content in industrial metals is second only to aluminum and iron. Magnesium alloy has the advantages of excellent specific strength, specific stiffness, damping and vibration reduction, dimensional stability, thermal conductivity, cutting processability, and easy recycling. Therefore, it has good application prospects in electronics, automobiles, and aerospace^[1,2].

When magnesium and its alloys are used as structural materials, the strength, rigidity, and wear resistance need to be further improved. The preparation of magnesium matrix composites (MMCs) by adding appropriate reinforcement phases to magnesium and its alloys can improve the performance to a certain extent. Compared with the matrix, the strength, modulus, damping performance, wear-resistance, and high temperature creep properties of MMCs have been improved to varying degrees. MMCs are another competitive light metal matrix composites after aluminum matrix composites (AMCs)^[3-7]. Compared with fiber-reinforced

MMCs and whisker-reinforced MMCs, particle-reinforced MMCs have a relatively simple preparation process, low production cost, good performance, and isotropy, making them the most widely used type of MMCs^[8]. The preparation technologies of particle reinforced MMCs mainly include powder metallurgy^[9-11], disintegrated melt deposition technique^[12,13], stir casting^[14-16], squeeze casting^[17,18] and friction stir processing^[19,20]. Compared to other methods, the stir casting method has the characteristics of easy operation, low cost, easy to achieve the near-net shape, which is the most suitable method for industrial production^[21]. But the main difficulties of this method are equally prominent. One of the biggest problems is how to obtain evenly distributed reinforcement particles. The wettability between matrix and reinforcement can be promoted by stirring. The stirring speed, stirring time, stirring temperature, the position of the stirring blade in the molten metal, and the volume fraction of the reinforcement all affect the distribution of the reinforcement. Stirring speed is one of the most significant process parameters.

The main factors to be considered in the selection of reinforcement phase for MMCs are as follows^[22,23]. (1) The reinforcement phase should have a high specific strength, high

Received date: February 23, 2022

Foundation item: National Natural Science Foundation of China (52171103); Guangdong Major Project of Basic and Applied Basic Research (2020B0301030006); Graduate Research and Innovation Foundation of Chongqing, China (CYB21001); Fundamental Research Funds for the Central Universities (2020CDJDPT001)

Corresponding author: Chen Xianhua, Ph. D., Professor, College of Materials Science & Engineering, Chongqing University, Chongqing 400045, P. R. China, Tel: 0086-23-65102633, E-mail: xhchen@cqu.edu.cn

Copyright © 2022, Northwest Institute for Nonferrous Metal Research. Published by Science Press. All rights reserved.

hardness, high elastic modulus, and high melting point. (2) The reinforcement phase needs to have a good thermal and chemical stability. (3) The compatibility between the reinforcement phase and the matrix is well, and it can form a good interface structure. The main particle reinforcement phases used in MMCs are ceramic particles, due to the high strength and modulus, good wear resistance as well as the high-temperature resistance, such as SiC, Al₂O₃, TiC, B₄C, and TiB₂ particles^[24-28].

Ceramic particles, as effective reinforcement phases used in MMCs, can improve the tribological properties, stiffness, hardness, and damping properties of MMCs. But the corresponding ductility will be sacrificed^[20]. Compared with ceramic particles, the metal reinforcement phase and the molten matrix alloy have better wettability, excellent ductility, and higher mechanical compatibility^[29]. By compositing magnesium and heterogeneous metals with high plasticity, high strength and high elastic modulus, metal strengthening particle may be achieved. It can realize the simultaneous improvement of strength and plasticity and opens a new way to improve the performance of magnesium alloys^[19, 29-33]. The mechanical deformation of Ti particles is several times higher than that of commonly used ceramic particles, so the Ti particles serve as a reinforcing phase that can help to improve the plasticity of the composites. Any intermetallic compounds will not form between titanium and magnesium, and they are both typical hexagonal crystal structure (hcp), which can alleviate the compatibility problem between reinforcement and matrix^[20].

In the present work, the effect of stirring speed on Ti_p/AM60 composites prepared by semi-solid stirring assisted ultrasonic vibration was investigated. The phase composition, distribution of Ti particles, element distribution at the interface of Ti particles, tensile properties, and strengthening mechanism of AM60 magnesium alloy reinforced by Ti particles were studied.

1 Experiment

1.1 Materials and processing

A commercial ingot of AM60 magnesium alloy was used as matrix with a chemical composition of 5.97wt% Al and 0.32wt% Mn. The irregular Ti particles with the particulate

size of 5~10 μm were used as reinforcements as shown in Fig.1.

Schematic diagram of the temperature-time sequences and experimental device for Ti_p/AM60 composites by semi-solid stirring assisted ultrasonic vibration are shown in Fig.2. First, under the protection of CO₂ and SF₆ atmosphere, about 1 kg of clean AM60 magnesium alloy was put into a crucible and melted in a resistance furnace at 720 °C, and then cooled to the stirring temperature of 610 °C, at which the AM60 matrix was in semi-solid state. Ti particles with a mass fraction of 2% were added into the semi-solid AM60 magnesium alloy. The stirring speeds were 300, 600 and 900 r/min, and the stirring time was 5 min. After stirring, the melt was increased to 650 °C and then ultrasonically processed for 10 min. The ultrasonic power remained at 500 W, and frequency was maintained at 20 kHz. After the ultrasonic treating, the melt was increased to 700 °C followed by the water cooling. In the end, Ti_p/AM60 composites were obtained. For comparison, the AM60 magnesium alloy without Ti particles was prepared with stirring speed of 300 r/min, and other preparation processes were the same.

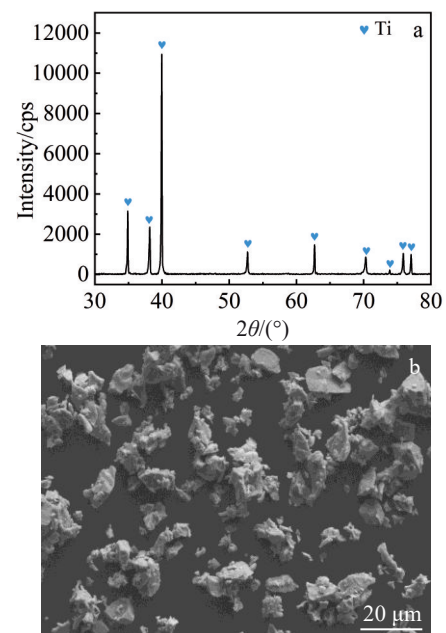


Fig.1 XRD pattern and SEM morphology of Ti particles

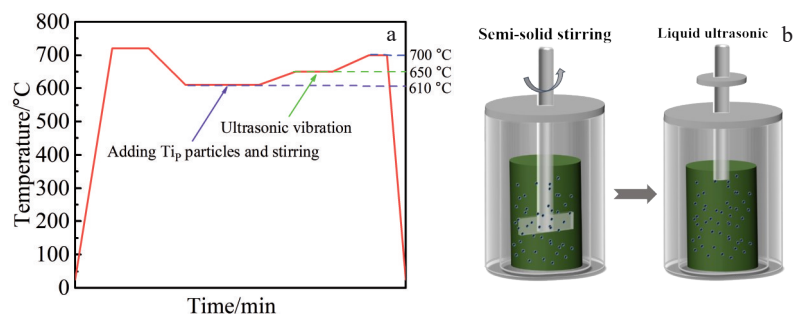


Fig.2 Schematic diagram of the temperature-time sequences (a) and experimental device (b) for Ti_p/AM60 composites by ultrasonic vibration assisted semi-solid stirring

1.2 Microstructure characterization

Small specimens (3 mm×5 mm×7 mm) cut from cast Ti_p/AM60 composites were hand-polished with 200#, 400#, 600#, 800# and 1000# SiC paper and then cleaned with ethyl alcohol. The phase composition of the specimens was measured by X-ray diffraction (XRD, Rigaku D/MAX-2500PC). Specimens for optical microscope (OM) and scanning electron microscope (SEM, JEOL JSM-7800F) observation were etched in 4% solution of HNO₃ in C₂H₅OH after being polished. OM was used to study the grain size of AM60 magnesium alloy and Ti_p/AM60 composites. SEM and EDS were used to study the distribution of Ti particles and elements at the interface of Ti particles. The interface structure between Ti particle and AM60 magnesium matrix was observed by transmission electron microscopy (TEM, FEI Talos F200x).

1.3 Tensile test

For assessing the tensile properties, the bone-shaped specimens with a gauge length of 15 mm and cross-section of 3 mm×6 mm were machined from the as-cast Ti_p/AM60 composites. A tensile test was performed at a tensile speed of 1 mm/min on a universal testing machine (GMT5105) at ambient temperature. The tests were repeated three times for each sample.

2 Results and Discussion

2.1 Phase compositions and microstructures

Fig. 3 shows the XRD patterns of prepared AM60 matrix alloy and the calculated section of the Mg-0.32Mn-xAl (wt%) phase diagram. The peaks of the AM60 matrix alloy are shown in Fig. 3a. It shows that the AM60 magnesium alloy is mainly composed of α -Mg and Mg₁₇Al₁₂ phases. The peak of the Mg₁₇Al₁₂ phase is slightly weaker in AM60 magnesium alloys with 6wt% Al. In addition, due to the presence of the Mn element, there will be the formation of Al-Mn-type intermetallic compound, and a weak peak of Al₈Mn₅ is detected. The calculated section of the Mg-0.32Mn-xAl (wt%) phase diagram is shown in Fig. 3b. Under equilibrium solidification conditions, with decreasing the temperature, the Al₈Mn₅ phase is crystallized in liquid AM60 magnesium alloy first, and then the α -Mg phase is crystallized until the liquid phase is wholly solidified into α -Mg and Al₈Mn₅ phases when x is equal to 6. Al₁₁Mn₄ phase and Al₄Mn phase are

precipitated gradually with the continuous decrease in temperature, and finally the microstructures at room temperature consist of α -Mg, Mg₁₇Al₁₂, and Al₄Mn phase. However, the actual solidification process is non-equilibrium solidification with a fast solidification rate. The Al₁₁Mn₄ phase and Al₄Mn phase cannot be precipitated in time, and only α -Mg, Mg₁₇Al₁₂, and Al₈Mn₅ phases are detected in the actual AM60 matrix alloy as shown in Fig. 3a.

Fig. 4 shows the XRD patterns of Ti_p/AM60 composites prepared at different stirring speeds. Besides α -Mg and Mg₁₇Al₁₂ components, the peak of Ti is detected at all three stirring speeds, which indicates that Ti particles are successfully added into the AM60 matrix alloy. The peak of Ti is relatively weak because the designed mass fraction of Ti particles is only 2wt%. The peak of the Al₈Mn₅ phase is difficult to detect. The alloying elements Ti and Al have an excellent chemical affinity with each other, and they are prone to form harmful compounds Ti-Al-type phase under high temperature and long-term contact, such as Ti₃Al^[9,10]. However, there is no peak of the Ti-Al-type phase in the XRD pattern after the addition of Ti particle, which may be due to insufficient exposure time during stir casting.

Solutes with good segregation ability and effective nucleation points are two essential factors for grain refinement. The solute segregation leads to the formation of a compositional supercooling region at the front of the liquid-solid interface, which hinders the growth of dendrites and provides the nucleation driving force of nucleation points in the compositional supercooling region. In addition, the nucleation ability of nucleation points determines the number of effective crystal nuclei in the compositional supercooling region before solidification.

Previous studies^[34-37] have demonstrated that the solute aggregation at the liquid-solid interface caused by the Al element and Mn element will affect the degree of subcooling of the alloy. After adding a certain amount of Mn element to the Mg-3Zn-0.2Ca (wt%) alloy, the grain size of the alloy decreases^[33]. The grain size of Mg-3%Al without Mn element is about 420 μ m, and it decreases to about 170 μ m after adding 0.2% Mn^[34]. After adding the Al element to Mg-6Zn-4Sn-1Mn alloy, the dendrites are gradually refined when the Al content increases^[35]. An optical micrograph of Ti_p/AM60 composites prepared at different stirring speeds is shown in

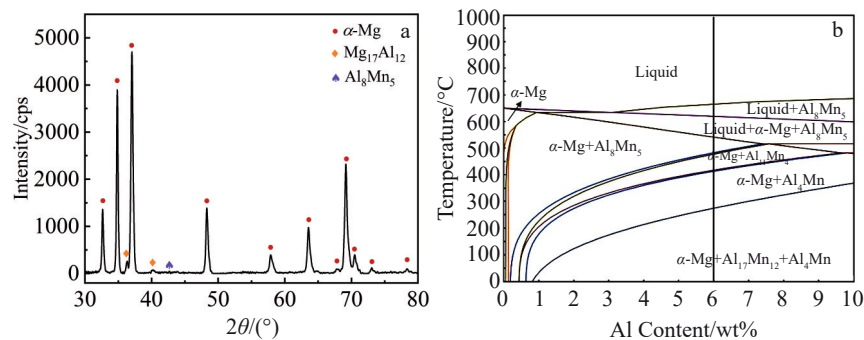


Fig. 3 XRD patterns of AM60 matrix alloy (a) and calculated section of the Mg-0.32Mn-xAl phase diagram (b)

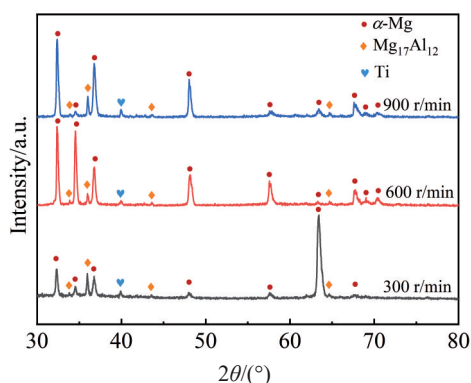


Fig.4 XRD patterns of $Ti_p/AM60$ composites with different stirring speeds

Fig.5. As can be seen, the grain size increases after adding Ti particles due to the decrease of Al and Mn content in the magnesium matrix. Under the same preparation conditions, the average grain size increases from 217 μm of pure AM60 magnesium alloy to 557 μm after adding Ti particles. And under the same Ti content, the change of average grain size is insignificant with the increase in stirring speed. It means that the change in grain size is mainly attributed to Ti particles.

Fig. 6 shows the SEM images of AM60 matrix alloy and $Ti_p/AM60$ composites prepared at different stirring speeds. The bright white phase is Ti particle. A certain amount of agglomeration still exists at the micro-scale. However, there is a particular gap between the Ti particles and they are not entirely agglomerated together, and large-scale agglomeration is not found on the macro-scale. The fine phase at the interface of the Ti particles is not the agglomerated Ti particles but the precipitated Al-Mn-type phase (Fig.7). There are many rod-like Al_8Mn_5 phases in AM60 matrix alloy as shown in Fig.6a. Compared with AM60 matrix alloy, the rod-

like Al_8Mn_5 phase in $Ti_p/AM60$ composites is reduced or disappears after adding Ti particles.

Moreover, Fig. 6b~6d reveal the distribution of Ti particles and the presence of pores near the Ti particles. The distribution of Ti particles can be affected by stirring speed. At higher stirring speeds, relatively large Ti particles are stirred into the matrix and fewer Ti particles are settled. Meanwhile, porosity increases with the increase in stirring speed. The microstructure shows that these pores mainly exist near Ti particles. The porosity in castings is principally caused by solidification shrinkage and dissolved gas in the melt^[38]. These pores observed in the $Ti_p/AM60$ composites are attributed to the hindered liquid metal flow caused by particle clustering, the pore nucleation at the Ti particles sites, the gas adsorbed on the surface of the Ti particles, the gas inhaled during stirring and the oxide film on the surface of the metal melt. More pores are observed in the microstructure at higher stirring speed, because vigorous stirring induces oxide inclusions, contaminants and gases into the melt.

Fig. 7a shows the SEM image of the interface between Ti particles and the Mg matrix. There are fine phases (2~3 μm) at the interface. The EDS analysis results show that the observed fine phase consists of aluminum and manganese (Fig. 7b~7f). The elemental mapping shows that the observed fine phase is close to the Al_8Mn_5 phase, which is compatible with the calculated results of the phase diagram in Fig. 3b. This result proves that Ti particles may act as a heterogeneous nucleation substrate for the Al_8Mn_5 phase. Furthermore, Fig. 7f indicates that a small amount of C element exists in the Ti particle, which may be due to the involved protective atmosphere CO_2 during the stirring process of preparation.

The interface characteristics between the magnesium matrix and the reinforcement will significantly affect the final mechanical properties of composites. In order to observe the

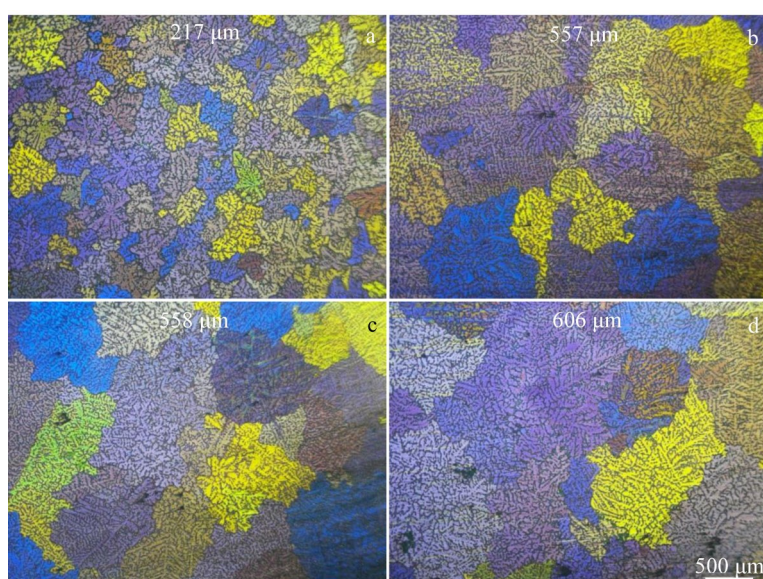


Fig.5 OM microstructures of AM60 matrix alloy and $Ti_p/AM60$ composites with different stirring speeds: (a) AM60, 300 r/min; (b) $Ti_p/AM60$, 300 r/min; (c) $Ti_p/AM60$, 600 r/min; (d) $Ti_p/AM60$, 900 r/min

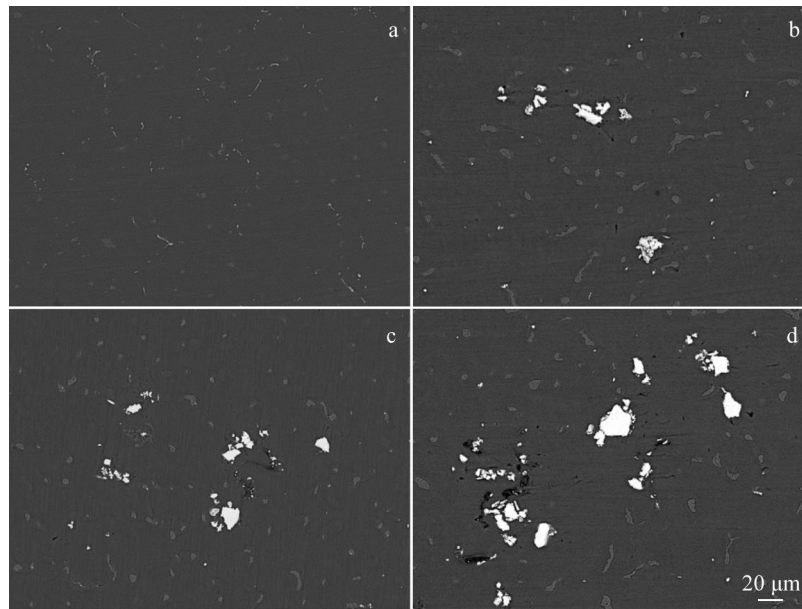


Fig.6 SEM images of AM60 matrix alloy and Ti_p/AM60 composites with different stirring speeds: (a) AM60, 300 r/min; (b) Ti_p/AM60, 300 r/min; (c) Ti_p/AM60, 600 r/min; (d) Ti_p/AM60, 900 r/min

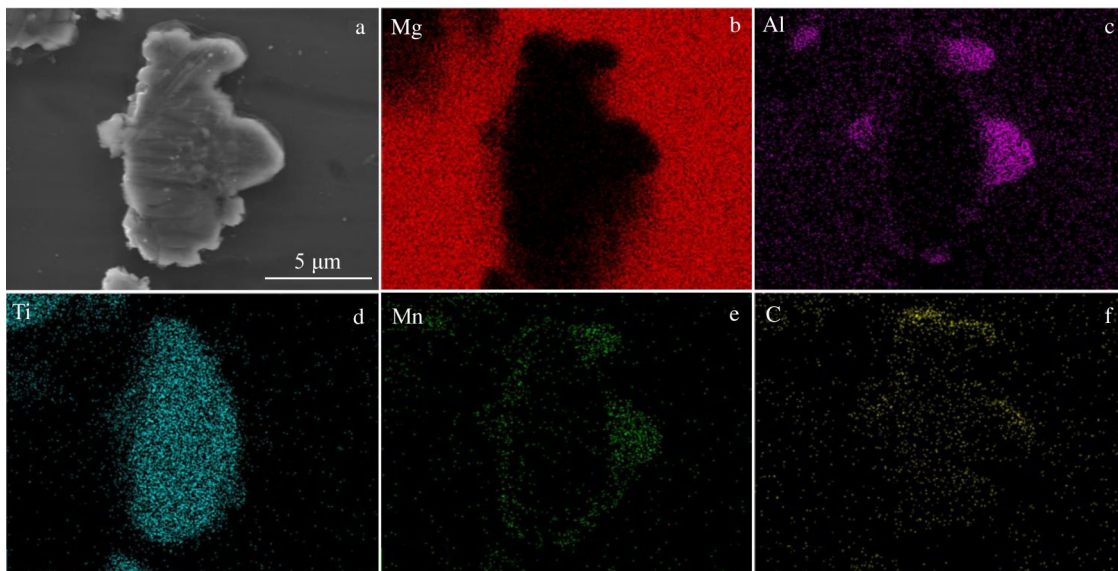


Fig.7 SEM image (a) and EDS mappings of interfacial elements (b-f) of Ti particle

interface structure between Ti particle and AM60 magnesium matrix more clearly, TEM images of Ti_p/AM60 composite are shown in Fig. 8. Fig. 8a shows some fine phases with size of 200~400 nm near the Ti particle. One fine phase is completely non-contact with the Ti particle, and the other is partially in contact with the Ti particle. Fig. 8b~8e show corresponding EDS mappings of the white block region in Fig. 8a. It can be seen from Fig. 8b and 8c that the gray area in the upper left corner is Ti particle, and the black area in the lower right corner is magnesium matrix. Fig. 8d and 8e show that the bright white particles in the lower right corner mainly contain the Al and Mn elements. Furthermore, the edge of the Ti particle contains both Al and Mn elements, which indicates

that Al atoms and Mn atoms are diffused from the Mg matrix to the edge of Ti particles during the preparation process. This diffusion leads to the decrease in the Al and Mn content in the Mg matrix, thus affecting the effect of Al and Mn elements on grain refinement, which is consistent with the results in Fig. 5.

Fig. 8f and 8g are the high-resolution transmission electron microscopy (HRTEM) images of the region A and B in Fig. 8a and the corresponding FFT patterns. The fine C and D phases are identified as Al₈Mn₅ phases, indicating that the Al₈Mn₅ phase not entirely precipitates near the Ti particles due to the Ti particles serving as the nucleation point of Al₈Mn₅. Another reason is that the thermal conductivity of Ti particles and the Mg matrix is quite different. The thermal conductivity of Mg

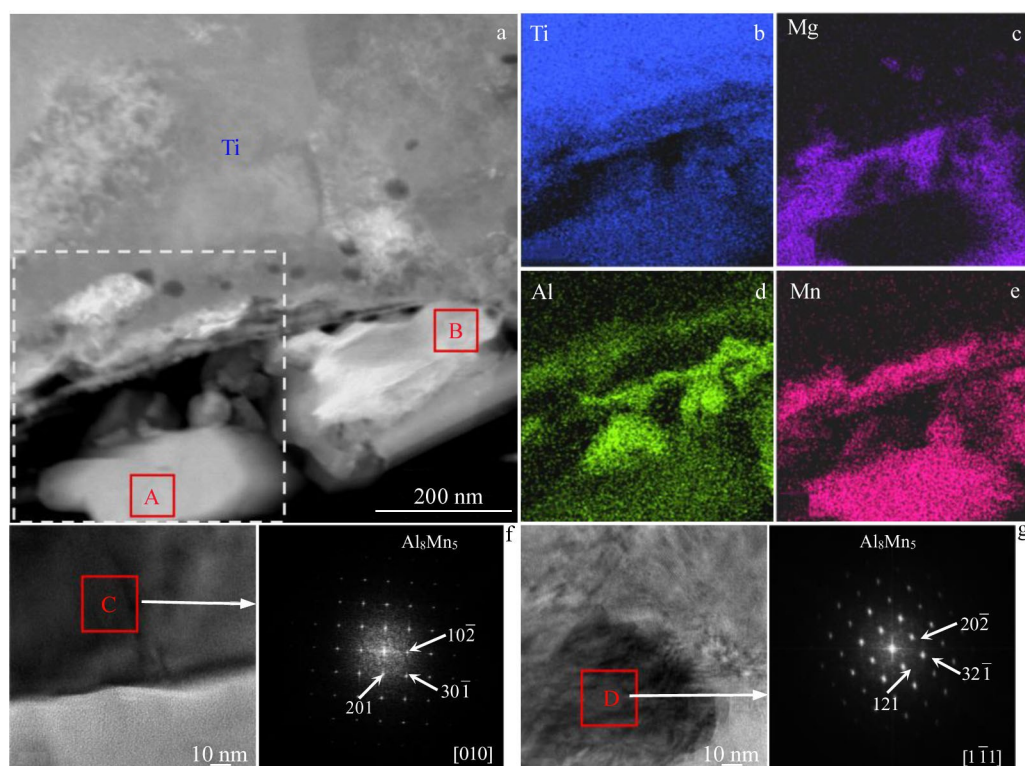


Fig.8 High-angle annular dark field (HAADF) image (a) and corresponding EDS mappings of white black region in Fig. 8a (b~e) for Ti/AM60 composites; HRTEM images and corresponding FFT patterns of region A ($\text{Al}_8\text{Mn}_5/\text{Mg}$ interface) (f) and region B (Ti/ Al_8Mn_5 interface) (g) marked in Fig. 8a

is about ten times larger than that of Ti. During the solidification of AM60 magnesium alloy, Al_8Mn_5 precipitates at about 660 °C (Fig. 3b). The temperature of the Mg matrix decreases rapidly, but near the Ti particles the temperature is relatively high, so the Al_8Mn_5 phase tends to precipitate near the Ti particles.

Previous research^[39] has shown that Al_8Mn_5 particles can serve as nucleation sites for primary magnesium grains in Mg-Al alloys. The Al_8Mn_5 phases precipitated at and near the interface of Ti particles are shown in Fig. 7 and Fig. 8, which reduce the uniformly distributed nucleation sites for primary magnesium grains in AM60 alloys, thus affecting the effect of Al_8Mn_5 phase on grain refinement. Therefore, the grain size of the AM60 alloy matrix increases after adding Ti particles due to the decrease in Al content, Mn content, and the Al_8Mn_5 phase in the magnesium matrix.

Consistent with Fig. 4, the peak of Al_8Mn_5 cannot be detected by X-ray due to the reduced content in the magnesium matrix.

Fig. 9 shows the line scanning area analysis of the Ti particle interface. The scanning direction is marked with a black arrow. Fig. 9c shows the HRTEM image of the line scanning area in Fig. 9a. The scanning line traverses four parts, marked as region 1, 2, 3 and 4 from Mg matrix to Ti particle. Fig. 9d shows an enlarged view of the white block in Fig. 9c. First, region 1 is the magnesium matrix. Then, the main elements in region 2 consist of Ti, Al, and Mn, which shows that the Al and Mn elements are diffused from the Mg matrix

to Ti particles. The ratio of Ti to Al in the middle of region 2 is about 3: 1, and the edge of region 2 mainly contains the Al element. According to the HRTEM analysis of region 2 of Fig. 9d, region 2 is the AlTi_3 phase. A small amount of Mg in region 2 may be introduced during sample preparation. Next, the main elements in region 3 consist of Al, Mn, and Ti. The ratio of Mn to Ti in the middle of region 3 is about 1: 1, and the edge of region 3 near region 2 mainly contains the Al element. It shows that much Al element is diffused into the boundary of region 2 and 3. The HRTEM analysis of region 3 of Fig. 9d proves that region 3 is the MnTi phase. Finally, region 4 is Ti particle.

There are three types of phase boundary structures: coherent interface, semi-coherent interface, and incoherent interface. The coherent interface has the lowest energy and the strongest interface bonding. Fig. 10 shows the interface structure between the Ti particle and the Al_8Mn_5 phase, and the interface structure between the Ti particle (AlTi_3 layer) and the magnesium matrix. It can be seen from Fig. 10a~10c that the coherent interface forms between the Ti particle and Al_8Mn_5 , which provides a theoretical basis that Ti particles can serve as a heterogeneous nucleation substrate for the Al_8Mn_5 phase. Due to the diffusion of Al and Mn atoms from the Mg matrix to the Ti particles, a MnTi layer and an AlTi_3 layer are formed at the edge of the Ti particles. Fig. 10d~10f show that a coherent interface form between the Ti particle (AlTi_3 layer) and Mg matrix, which is a strong interfacial bonding. During the deformation process, the strong interfacial bonding

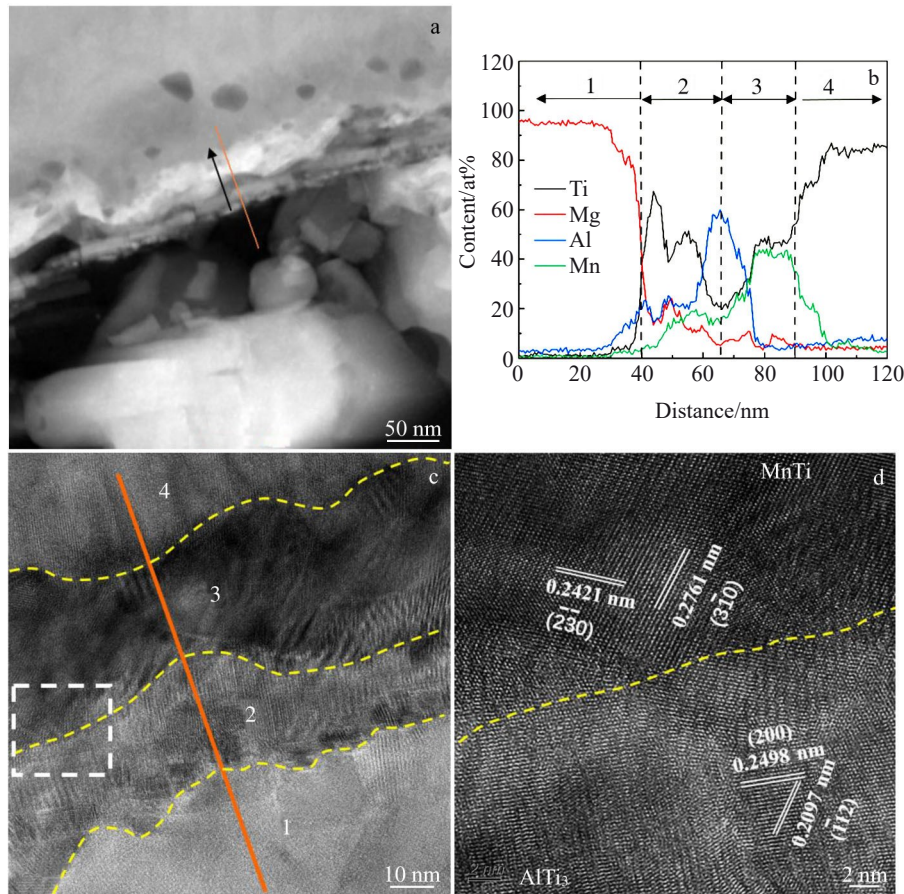


Fig.9 HAADF image (a) and EDS line scanning results along marked line (b); HRTEM images of line scanning region in Fig.9a (c) and MnTi/AlTi₃ interface (d)

facilitate the efficient transfer of loads from the Mg matrix to the Ti particles, contributing to tensile properties.

2.2 Mechanical properties

The uniaxial tensile test results of the as-cast Ti_p/AM60 composites are shown in Fig. 11. The YS decreases compared with that of AM60 matrix alloy since the magnesium matrix grain is coarsened after adding Ti particles. At the same time, the UTS and elongation both increase after adding Ti particles to the AM60 matrix alloy compared to the values of the AM60 matrix alloy.

Under the same preparation conditions, UTS increases from 159 MPa of pure AM60 magnesium alloy to 172 MPa, and elongation is also improved from 9.5% to 12% after adding Ti particles. The flow mode of the molten metal after adding the Ti particles is directly affected by the Ti particles and the stirring speed. With the same Ti content, the UTS and elongation both increase first and then decrease with the increase in the stirring speed. The stirring speed of 300 r/min is not enough to disperse Ti particles, which makes the agglomeration of part Ti particles relatively more severe, thus affecting the effect of Ti particles on mechanical property. Therefore, the improvement in UTS is not significant under lower stirring speed. When the stirring speed is improved to 600 r/min, UTS increases from 172 MPa to 183 MPa, and

elongation is improved from 12% to 14.3%. It means that the distribution of Ti particles can be improved by increasing the stirring speed, thus reducing the negative impact of particle agglomeration on mechanical property. However, when the stirring speed reaches to 900 r/min, the vortex is prone to form due to vigorous stirring. It will increase the porosity content and oxidized inclusions in Ti_p/AM60 composites during smelting and reduce the mechanical properties.

In this study, the enhancement effect of Ti particles is partly offset by grain coarsening. So the strengthening mechanism of AM60 magnesium alloy reinforced by Ti particles is as follows^[6,7,40]: (i) dislocation strengthening; (ii) second phase strengthening; (iii) load-bearing effects. After introducing the reinforcing phase Ti particles, the mismatch of elastic modulus and the thermal expansion coefficient between AM60 matrix and Ti particles lead to the increase in dislocation density in Ti/AM60 composites. The thermal expansion coefficient of AM60 magnesium alloy is generally larger than that of Ti particles^[31], which will cause residual stress in the composites. Therefore, during the preparation process, plastic deformation may occur in AM60 magnesium alloy, resulting in the formation of high-density dislocations to produce a strengthening effect. The Ti particles are dispersed in the matrix and can be regarded as the second phase when

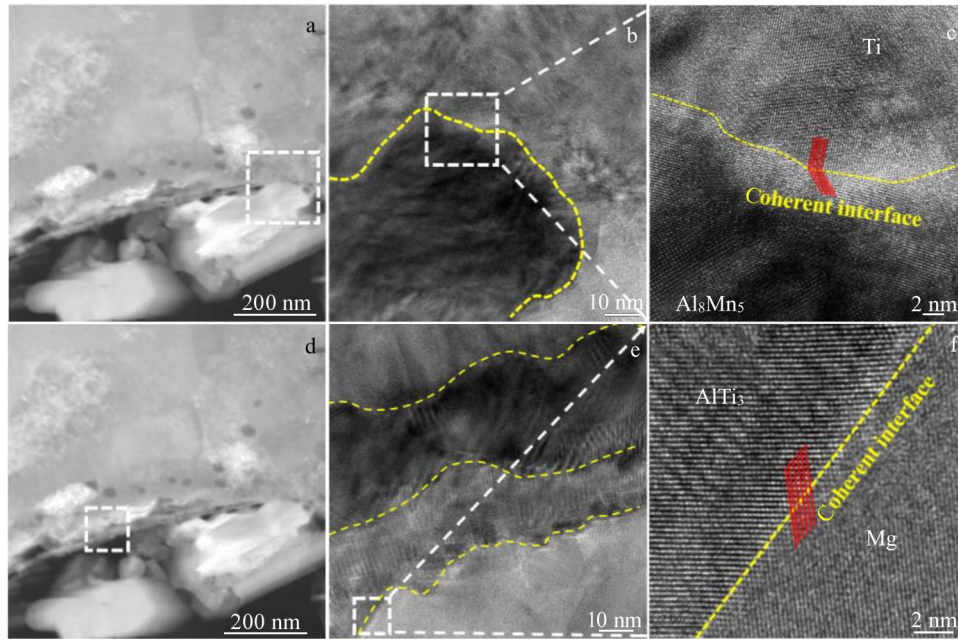


Fig.10 HAADF images of the interface of Ti particle and corresponding HRTEM images: (a~c) Ti/Al₈Mn₅ and (d~f) Ti/Mg

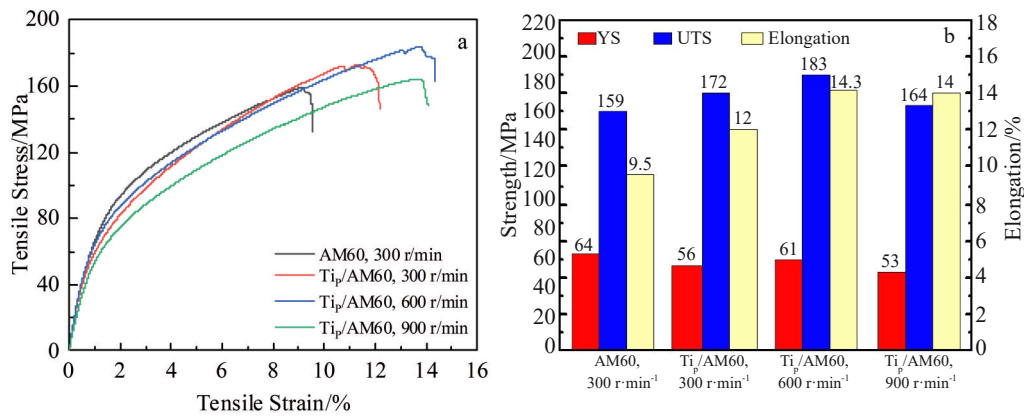


Fig.11 Stress-strain curves of Ti_p/AM60 composites (a) and extracted values (b)

the size of some introduced Ti particles is less than 1 μm . Ti particles hinder the slippage of the dislocations in the matrix and generate the accumulation of dislocations, thereby improving the strength of the matrix. When materials are subjected to vertical load, Ti particles, as the reinforcing phase, share part of the load of the matrix.

The toughening mechanism of Ti_p/AM60 composites is the deformability of Ti particles. Ti particles have excellent ductility, higher mechanical compatibility, and better wettability with molten matrix alloy compared with ceramic particles. In previous studies^[20, 41], the strength of MMC reinforced with Ti particles prepared by friction stir processing and powder metallurgy is improved, but the ductility is relatively reduced after adding Ti particles. In this work, the elongation is improved after adding Ti particles. The reasons are as follows. The excellent wettability between the Mg matrix and the Ti particles in the composites prepared by the stir casting method can be achieved. The excellent

interface structure finally forms between the Ti particles and Mg matrix. A strong interfacial bonding delays the debonding of the Ti particles and Mg matrix during the deformation process, which is contributed to plasticity improvement.

3 Conclusions

- 1) In Ti_p/AM60 composites, Al and Mn elements have an effect of grain refinement. Therefore, the reduction of Al and Mn element content in the Mg matrix results in grain size increase after adding Ti particles.
- 2) A strong interfacial bonding of coherent interface can be formed between Ti particles (AlTi₃ layer) and the Mg matrix. The strong interfacial bonding facilitates the efficient transfer of loads from the Mg matrix to the Ti particles during the deformation process.
- 3) The UTS and elongation increase after adding Ti particles to AM60 magnesium alloy compared to those of AM60 matrix alloy. The strengthening mechanism of AM60

magnesium alloy reinforced by Ti particles mainly includes dislocation strengthening, second phase strengthening, and load-bearing effects.

4) With increasing the stirring speed, the UTS and elongation both increase first and then decrease. When the stirring speed is 600 r/min, the maximum UTS and elongation reach 183 MPa and 14.3%, respectively.

References

- Wang Q H, Jiang B, Chen D L et al. *Journal of Materials Science*[J], 2021, 56: 12 965
- Peng Peng, Tang Aitao, Wang Bo et al. *Journal of Materials Research and Technology*[J], 2021, 15: 1252
- Dinakaran I, Vettivel S C, Balakrishnan M et al. *Journal of Magnesium and Alloys*[J], 2019, 7(1): 155
- Bommala Vijay Kumar, Krishna Mallarapu Gopi, Rao Ch Tirumala. *Journal of Magnesium and Alloys*[J], 2019, 7(1): 72
- Ma Guohong, Xiao Hao, Ye Jia et al. *Materials Science and Technology*[J], 2020, 36(6): 645
- Zhu Junwen, Jiang Wenming, Li Guangyu et al. *Journal of Materials Processing Technology*[J], 2020, 283: 116 699
- Jiang Wenming, Zhu Junwen, Li Guangyu et al. *Journal of Materials Science & Technology*[J], 2021, 88: 119
- Liao Wenjun, Ye Bing, Zhang Li et al. *Materials Science and Engineering A*[J], 2015, 642: 49
- Yu Huan, Sun Yu, Hu Lianxi et al. *Materials Characterization*[J], 2017, 127: 272
- Yu Huan, Sun Yu, Wan Zhipeng et al. *Journal of Alloys and Compounds*[J], 2018, 741: 231
- Wu Bo, Li Jianbo, Ye Junliu et al. *Vacuum*[J], 2021, 183: 109 833
- Ho K F, Gupta M, Srivatsan T S. *Materials Science and Engineering A*[J], 2004, 369(1-2): 302
- Meenashisundaram Ganesh Kumar, Gupta Manoj. *Journal of Alloys and Compounds*[J], 2014, 593: 176
- Nie Kaibo, Guo Yachao, Munroe Paul et al. *Journal of Alloys and Compounds*[J], 2020, 819: 153 348
- Rao Thella Babu. *Materials Science and Engineering A*[J], 2021, 805: 140 553
- Sunu Surendran K T, Gnanavelbabu A. *Materials Today: Proceedings*[J], 2021, 45: 7845
- Surendran K T Sunu, Gnanavelbabu A, Rajkumar K. *Materials Today: Proceedings*[J], 2021, 45: 7822
- Gnanavelbabu A, Surendran K T Sunu, Loganathan P et al. *Journal of Alloys and Compounds*[J], 2021, 856: 158 173
- Dinakaran Isaac, Zhang Shuai, Chen Gaoqiang et al. *Journal of Alloys and Compounds*[J], 2020, 820: 153 071
- Dinakaran Isaac, Zhang Shuai, Chen Gaoqiang et al. *Materials Science and Engineering A*[J], 2020, 772: 138 793
- Huang Song-Jeng, Abbas Aqeel. *Journal of Alloys and Compounds*[J], 2020, 817: 153 321
- Braszczyńska K N. *Ztschrift fur Metallkunde*[J], 2013, 94(2): 144
- Mortensen Andreas, Llorca Javier. *Metal Matrix Composites*[J], 2010, 40: 243
- Zhu Juanjuan, Qi Jiahui, Guan Dikai et al. *Tribology International*[J], 2020, 146: 106 253
- Azizieh M, Kokabi A H, Abachi P. *Materials & Design*[J], 2011, 32(4): 2034
- Peter Pushpanathan D, Alagumurthi N, Pradeep Devaneyan S. *Materials Today: Proceedings*[J], 2020, 22: 2565
- Liu Ruifeng, Wang Wenxian, Chen Hongsheng et al. *Journal of Alloys and Compounds*[J], 2019, 788: 1056
- Xiao Peng, Gao Yimin, Xu Feixing et al. *Tribology International*[J], 2018, 128: 130
- Braszczyńska-Malik K N, Przełoczyńska E. *Journal of Alloys and Compounds*[J], 2018, 731: 1181
- Kondoh Katsuyoshi, Kawakami Masashi, Imai Hisashi et al. *Acta Materialia*[J], 2010, 58(2): 606
- Hassan S F, Gupta M. *Journal of Alloys and Compounds*[J], 2002, 345: 246
- Pérez P, Garcés G, Adeva P. *Composites Science and Technology*[J], 2004, 64(1): 145
- Braszczyńska-Malik K N, Przełoczyńska E. *Journal of Alloys and Compounds*[J], 2017, 728: 600
- Cho Dae Hyun, Lee Byoung Woo, Park Jin Young et al. *Journal of Alloys and Compounds*[J], 2017, 695: 1166
- Han Yuyan, You Chen, Zhao Yun et al. *Frontiers in Materials*[J], 2019, 6: 324
- Cao Peng, Qian Ma, StJohn David H. *Scripta Materialia*[J], 2006, 54(11): 1853
- Hou Caihong, Ye Zhisong, Qi Fugang et al. *Transactions of Nonferrous Metals Society of China*[J], 2021, 31(7): 1951
- Ilegbusi J Olusegun, Yang Jijin. *Metallurgical and Materials Transactions A*[J], 2000, 31: 2069
- Sonsino C M, Dieterich K, Wenk L et al. *Magnesium Alloys and Their Applications*[M]. New York: John Wiley & Sons, Ltd, 2000
- Gupta M, Mui N, Ling S. *Magnesium, Magnesium Alloys, and Magnesium Composites*[M]. New York: John Wiley & Sons, Ltd, 2010
- Yu Huan, Zhou Haiping, Sun Yu et al. *Advanced Powder Technology*[J], 2018, 29(12): 3241

Ti_p/AM60 复合材料的组织与力学性能

蒲冬梅¹, 陈先华^{1,2}, 叶俊镠¹, 刘春全¹, 赵 杰¹, 潘复生^{1,2}

(1. 重庆大学 材料科学与工程学院, 重庆 400045)

(2. 国家镁合金工程技术研究中心, 重庆 400045)

摘 要: 采用超声振动辅助半固态搅拌法在不同搅拌速度下制备了钛颗粒增强 AM60 镁基复合材料。显微组织结果表明, 加入 Ti 颗粒后, 晶粒尺寸增大, Ti 颗粒界面处析出 Al₈Mn₅ 相, Ti 颗粒与 Mg 基体的界面结构为结合良好的共格界面。拉伸试验结果表明, Ti_p/AM60 复合材料的抗拉强度高于 AM60 镁合金基体。随着搅拌速度从 300 r/min 增加到 900 r/min, 抗拉强度和伸长率均先增大后减小。当搅拌速度为 600 r/min 时, Ti_p/AM60 复合材料的抗拉强度和伸长率分别达到最大值 183 MPa 和 14.3%。与 AM60 基体合金相比, 复合材料的抗拉强度提高了 15%, 延伸率提高了 51%。

关键词: 镁基复合材料; Ti 颗粒; 半固态搅拌; 拉伸性能

作者简介: 蒲冬梅, 女, 1995 年生, 博士, 重庆大学材料科学与工程学院, 重庆 400045, E-mail: 20200901059@cqu.edu.cn